Pinning of fluid membranes by periodic harmonic potentials

N. Gov and S. A. Safran
Department of Materials and Interfaces, The Weizmann Institute of Science, P.O. Box 26, Rehovot, Israel 76100
(Received 27 May 2003; published 13 January 2004)

We analyze the thermal fluctuations of fluid membranes in the presence of periodic confining harmonic potentials. This is a simple model of the biologically important, inhomogeneous attachment of the cytoskeleton to the external, fluid membrane of the cell. We study a two-dimensional checkerboard potential as well as one-dimensional, sinusoidal and periodic highly localized, δ function potentials. The membranes are described by an energy functional that includes the curvature bending modulus of the membrane and the harmonic external potential. We predict the magnitude of the membrane shape fluctuations. The sinusoidal potentials give a spontaneous surface tension, and an emergent intermediate-range order in the membrane undulations. The δ function potentials induce a renormalization of the curvature modulus, with perfect pinning at the δ potential sites. After spatial averaging, the δ-function potentials also give rise to an effective surface tension. Finally, we compare these results with measurements of the fluctuations of the red-blood cell membrane, which shows the effects of cytoskeleton attachment to the cellular membrane.

DOI: 10.1103/PhysRevE.69.011101 PACS number(s): 05.40.−a, 05.65.+b

I. INTRODUCTION

The coupling between the elastic cytoskeleton and the fluid, lipid membrane is important for understanding the mechanical properties and fluctuation spectrum of the cell. The details of the cytoskeleton components and its geometry vary between cells, but there are general features that are common to all: the fluid bilayer is attached to the cytoskeleton through specialized membrane proteins, confined to small attachment patches of $\sim$10–50 nm each, which can be relatively sparse ($\sim$100 nm apart in the red-blood cell (RBC) [1], Fig. 1). The cytoskeleton itself is usually much stiffer than the bilayer, and its solidlike structure gives it a shear modulus. The part of the bilayer that is attached to the cytoskeleton is therefore highly confined with respect to fluctuations in the normal and lateral directions. It is interesting to see how this highly inhomogeneous confinement affects the entire membrane, including those sections that are not directly attached to the cytoskeleton.

In this paper we focus on the effects of the inhomogeneous confinement on the thermal fluctuations of the membrane. These fluctuations have been measured in RBC's [2], and the effective membrane bending modulus κ was found to vary dramatically as a function of the measurement wave vector q. These observations, as well as the temporal spectrum [3], have presented a theoretical challenge since they appear to indicate that the bilayer behaves as if it is almost detached from the underlying cytoskeleton [4,5]. In our previous work [5] we have introduced a phenomenological model that describes the cytoskeleton influence on the bilayer fluctuations in terms of a uniform harmonic confinement (described by the parameter γ). At the same time, the membrane appears to acquire a wavelength-dependent surface tension stiffness, in addition to its curvature modulus [5,19]. This tension is much larger than estimated from the finite size effect [6] $\sigma \gg \kappa/R^2$. The aim of the present work is to calculate rigorously the effects of the nonuniform coupling of the cytoskeleton to the bilayer (Fig. 1), on the bilayer thermal fluctuations. Using this calculation we obtain a microscopic justification for the phenomenological model of Ref. [5], and the confinement and surface tension parameters γ and σ, respectively. In the present work we predict these properties using a simple, well controlled model. Our aim here, therefore, is not necessarily to improve on the quality of the fit that was already obtained in Ref. [5], but to motivate the use of the phenomenological parameters and to relate them to the microscopic nature of the cytoskeleton-bilayer coupling, with particular focus on its inhomogeneous, sparse structure.

Our simplified model approximates the membrane-cytoskeleton coupling as a confining harmonic potential, placed periodically along the membrane. The point of attachment of the cytoskeletal spectrin network to the membrane is through relatively short and rigid protein complexes [1] (p. 4.1, p. 55, etc). It is the flexible spectrin filaments that provide the smooth restoring force of the cytoskeleton on the membrane, which can be treated harmonically. The spectrin molecules behave as linear entropic springs, with nonlinearity at large extensions [7], beyond the range of the thermal fluctuations which we discuss here (Fig. 1). We study two extreme modes of the lateral potential: a series of δ functions, and a smooth sinusoidal function. For both cases we find analytical solutions for a one-dimensional membrane,

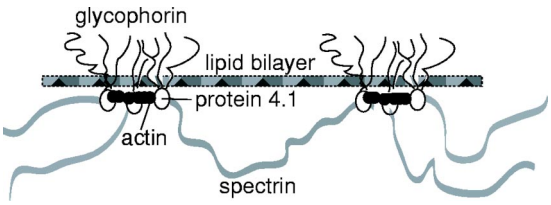

FIG. 1. Schematic illustration of the components of the RBC membrane and cytoskeleton. Not shown are the additional connections between the spectrin filaments (gray ribbons) and the lipid bilayer (dashed filled rectangle) through randomly placed ankryn complexes, which do not modify the network connectivity. The flat bilayer drawn is where the plane of zero displacement $h=0$ is defined.

and for the sinusoid we also calculate the fluctuations for the two-dimensional case.

The qualitative effects of the inhomogeneous confinement are the spontaneous appearance of a surface tension, which is significantly larger than that given by the finite size effect, and a uniform confinement term. For the case of a weak sinusoidal confinement we also find enhanced correlations at a characteristic length scale, due to ''interference'' effect of neighboring confinement peaks. This occurs when the persistence length of the membrane is larger than the harmonic potential periodicity.

We finally compare the results of our model calculations with the measurements of the fluctuations of the RBC membrane. This membrane is attached to a two-dimensional (roughly) triangular cytoskeleton—the spectrin network [1] (Fig. 1). We find that our calculation can reproduce the effect of the uniform confinement and the appearance of an effective surface tension, as found in the experiments. Previously [5] these parameters were fitted individually from the experimental data. Through the present calculation these parameters can be related to the microscopic properties of the cytoskeleton; the periodicity of the connections and the strength of the attachments (see Sec. III for details, Fig. 1).

II. MODEL

In this work we use the connection between thermal averages and fluctuations, to calculate the effect of a periodic confining potential on the shape fluctuations of a membrane.

We begin with the definition of the thermal average of the normal displacement h of the membrane at site i [6],

$$\langle h_i \rangle = \frac{1}{Z} \int d\Lambda e^{-H/k_B T} h_i , \tag{1}$$

where the partition function $Z = \int d\Lambda e^{-H/T}$ and $d\Lambda$ is the phase-space integral. The Hamiltonian H of the membrane is given by

$$H = \int \frac{\kappa}{2} (\nabla^2 h)^2 dr + \frac{1}{2} \int V(r - r') h(r) h(r') dr\, dr', \tag{2}$$

where κ is the bending modulus and $V(r-r')$ is the external potential that represents the inhomogeneous coupling to the cytoskeleton. For a locally acting, harmonic confining potential, the second term in Eq. (2) becomes $V(r)h(r)^2$. To calculate the correlations, we can introduce a fictitious field f to the free energy [6], which couples linearly to the normal displacement (linear response approximation). This adds the following term to the Hamiltonian

$$H_f = H - \int f \delta(r) h(r) dr. \tag{3}$$

Taking the derivatives with respect to f, we find that the height-height correlation is [6]

$$\langle [h(0) - \langle h(0) \rangle] h(r) - \langle h(r) \rangle] \rangle = -k_B T \left. \frac{\partial \langle h(r) \rangle}{\partial f} \right|_{f=0} . \tag{4}$$

where $\langle h(r) \rangle \equiv \chi(r)$ is the average membrane deviation in the presence of the field f (being zero otherwise). In a mean-field type of approximation, this average is the solution to the energy minimization (Euler-Lagrange) equation

$$\frac{\partial H_f}{\partial h} = 0 \Rightarrow V(r)\chi(r) + \kappa \nabla^4 \chi(r) = f \delta(r), \tag{5}$$

where $\chi(r) = \langle h(r) \rangle$ is the mean-field value of the normal displacement of the membrane.

This model therefore describes a membrane that is free to fluctuate around its average position $h=0$ (Fig. 1). The harmonic confinement acts symmetrically on the membrane, even though the physical cytoskeleton is attached to only one side of the lipid membrane. The asymmetry in the real membrane fluctuations becomes important only for large fluctuations where the membrane ''hits'' the spectrin filaments and makes the network break or buckle. These large deformations are beyond the range of this linear model. We further note that one should average over the location of the fictitious field f with respect to the harmonic potentials. The reason for this is that experiments on real membranes [2] lack the resolution to distinguish between the bilayer regions that are attached to the underlying cytoskeleton. Furthermore, the membranes are fluid, so that the cytoskeleton-bilayer coupling sites fluctuate in the plane of the membrane. Therefore after calculating the correlation functions, we average over the positions of the harmonic potentials, keeping the location of the field f at the origin.

The Fourier transform of the energy minimization equation is

$$\sum_G V_G \chi_{q-G} + \kappa q^4 \chi_q = f. \tag{6}$$

Since χ_q is linear in f, we see from Eq. (4) that χ_q is simply proportional to the Fourier transform of the two-point correlation function. For a free membrane ($V_G = 0$), we have from Eq. (6) $\chi_q = f/\kappa q^4$. Transforming this back to real (two-dimensional) space we recover in the limit of a large membrane of size L (the complete result is in Appendix A) the well-known self-correlation (in the limit $r \to 0$)

$$\langle h(0) h(r \to 0) \rangle \simeq \frac{k_B T L^2}{4\pi\kappa}. \tag{7}$$

For any external potential it is possible to solve Eq. (6) numerically. In order to obtain analytic expressions, we will make a series of simplifications and approximations, later comparing the results with the numerical solutions.

In the presence of a uniform external potential V (where only $V_{G=0}$ is nonzero) the solution takes the following form (5):

$$\chi_q = \frac{f}{\gamma + \kappa q^4}, \tag{8}$$

where $\gamma = V_{G=0}$. Transforming Eq. (8) back to real (two-dimensional) space we find for the self-correlation

$$\langle h(0)h(0)\rangle = \frac{k_B T}{8\sqrt{\kappa\gamma}} \tag{9}$$

which shows clearly the effect of uniform confinement, compared to the free membrane result (7).

III. SINUSOIDAL POTENTIAL

The differential equation (6), for a periodic potential characterized by a single wave vector $\pm G$ $(G \neq 0)$, gives an infinite series of algebraic equations [8]. In analogy with the solution of the electronic wave equation in a periodic potential [8], we approximate the infinite series of algebraic equations (6) by keeping only the first-order terms in G. Since we expect (and later find) the amplitude χ_q to decay with increasing q, we expand up to first order in G, i.e., $G \gg q$. This amounts to the assumption that only the first-order scattering of the membrane undulations by the periodic potential contributes significantly.

We now calculate χ_q for a two-dimensional checkerboard potential of the form $V(x,y) = V_1 + V_0 \cos(Gx)\cos(Gy)$, where the sinusoidal harmonic potential of amplitude V_0 is superimposed on the uniform background of amplitude $V_1 \geqslant V_0$. This potential should physically resemble the confining of the sparse network of the RBC cytoskeleton (see the following section). We therefore write

$$[V_1 + \kappa(q_x^2 + q_y^2)^2]\chi_q + \frac{V_0}{4} e^{i\delta_x} e^{i\delta_y} \chi_{G+q_x, G+q_y} + \frac{V_0}{4} e^{-i\delta_x} e^{i\delta_y} \chi_{-G+q_x, G+q_y} + \frac{V_0}{4} e^{i\delta_x} e^{-i\delta_y} \chi_{G+q_x, -G+q_y} + \frac{V_0}{4} e^{-i\delta_x} e^{-i\delta_y} \chi_{-G+q_x, -G+q_y} = f,$$

$$\frac{V_0}{4} e^{-i\delta_x} e^{-i\delta_y} \chi_q + \{V_1 + \kappa[(G+q_x)^2 + (G+q_y)^2]^2\} \times \chi_{G+q_x, G+q_y} = f,$$

$$\frac{V_0}{4} e^{i\delta_x} e^{-i\delta_y} \chi_q + \{V_1 + \kappa[(-G+q_x)^2 + (G+q_y)^2]^2\} \times \chi_{-G+q_x, G+q_y} = f,$$

$$\frac{V_0}{4} e^{-i\delta_x} e^{i\delta_y} \chi_q + \{V_1 + \kappa[(G+q_x)^2 + (-G+q_y)^2]^2\} \times \chi_{G+q_x, -G+q_y} = f,$$

$$\frac{V_0}{4} e^{i\delta_x} e^{i\delta_y} \chi_q + \{V_1 + \kappa[(-G+q_x)^2 + (-G+q_y)^2]^2\} \times \chi_{-G+q_x, -G+q_y} = f. \tag{10}$$

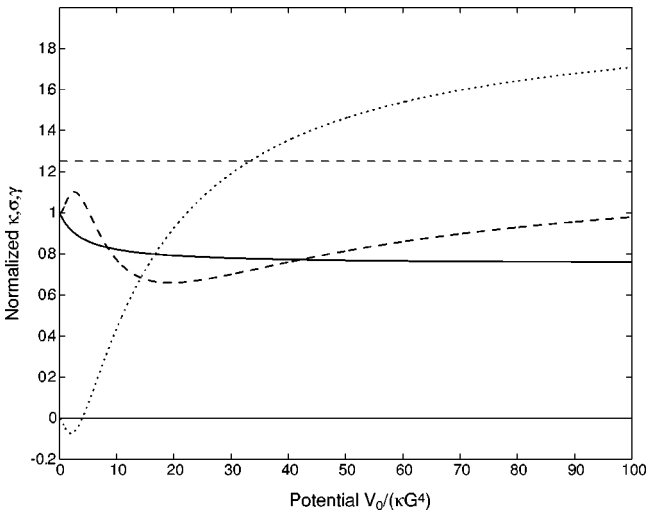

FIG. 2. Analytic expressions for the effective $\overline{\kappa}/\kappa$ (dashed line), $\overline{\sigma}/(\kappa G^2)$ (dotted line), $\overline{\gamma}/V_0$ (solid line), Eq. (A4), for the checkerboard potential. The horizontal dashed line at 5/4 shows the limit of $\overline{\kappa}/\kappa$ for $V_0 \to \infty$.

The shifts of the sinusoidal functions with respect to the origin (where the force f is applied) $0 < \delta_x, \delta_y < 2\pi$ are averaged over at the end of the calculation, since we are interested in the translationally invariant response (this procedure does not make any qualitative changes). We solve Eqs. (10) exactly, that is, χ_q for the two-dimensional checkerboard potential. Since the resulting expressions are long, it is more manageable to look at the behavior along one particular direction. We give in Appendix A the result for χ_{q_x} (a cut along $q_y = 0$), while for simplicity we take $V_1 = V_0$ [Eq. A3].

We next compare the solution of the analytical calculation [Eqs. (10) and (A3)] with a numerical solution of up to fourth order (i.e., $\pm 4G$). The average discrepancy is $\pm 2\%$ for $V_0 = \kappa G^4$, which grows to $\sim 10\%$ for $V_0 = 10\kappa G^4$. The analytical results are therefore less accurate for larger harmonic potentials, or small G. Indeed, we assumed in deriving Eq. (10) that G is large enough so that only the nearest neighbors in q space need to be taken into account.

Expanding Eq. (A3) up to fourth order in q we can define the effective bending modulus $\overline{\kappa}$, surface tension $\overline{\sigma}$, and the uniform ("Helfrich") confinement parameter $\overline{\gamma}$ (A4), as the coefficients of q^4, q^2, and q^0, respectively, in the expression for χ_q^{-1}. We plot these quantities in Fig. 2 as functions of the ratio $V_0/G^4\kappa$. Note the spontaneous appearance of a surface tension term [9].

We find that these quantities (A4) have the following behavior in the limit of both weak ($\epsilon^{-1}=V_0/G^4\kappa \ll 1$) and strong ($\epsilon^{-1}=V_0/G^4\kappa \gg 1$) confinement:

$$V_0\to 0:\ \overline{\gamma}\to V_0,\quad \overline{\sigma}\to -\frac{V_0^2}{8G^6\kappa},\quad \overline{\kappa}\to\kappa,$$

$$V_0\to\infty:\ \overline{\gamma}\to\frac{3V_0}{4},\quad \overline{\sigma}\to 2\kappa G^2,\quad \overline{\kappa}\to\frac{5}{4}\kappa. \qquad (11)$$

For weak confinement, both the curvature modulus and the uniform confinement γ are easily understood; however we find a surprising effective *negative* surface tension for weak potentials $V_0<4\kappa G^4$. In the limit of strong confinement we find that the surface tension saturates to a positive value that is much larger than the tension due to finite size effects, with a renormalized bending modulus and monotonically increasing uniform confinement (Fig. 2).

In both cases it is the ''pulling'' effect of the inhomogeneous pinning that induces the appearance of the effective surface tension. In the limit $V_0\to\infty$, the clamping has a similar effect to positive σ that tends to reduce the fluctuations. In the limit $V_0\to 0$, there appears a characteristic wave vector q_0 (see below), which is similar to the effect of buckling that a negative tension would induce.

The renormalization of the bending modulus to a value of $5/4\kappa$ (11) is somewhat similar to the effects calculated for membranes with grafted polymers and brushes [10], where factors of 3/2–5/2 have been found. The similarity is clear, as the grafted molecules apply a smooth entropic constraint on the membrane fluctuations, similar to the harmonic potential that we are applying here.

The effective negative surface tension for small V_0 (Fig. 2) means that there is a peak in the correlation function χ_q (A3), at some finite wave vector q_0. The appearance of a typical wavevector, even after averaging over the sinusoidal potential position, is surprising. Using the expansion of χ_q up to fourth order in q, we find an approximate expression for this wavevector q_0 (Eq. (A5) in Appendix A)

$$q_0=\begin{cases} G(V_0/4G^4\kappa), & V_0\to 0 \\ \dfrac{(V_c-V_0)^{1/2}}{\sqrt{34\kappa}G}, & V_c-V_0\to 0, \end{cases} \qquad (12)$$

where $V_c=4\kappa G^4$. In Fig. 3 we plot this function. There is no real solution for $V_0>V_c$, which corresponds to the regime of positive surface tension $\overline{\sigma}$ (Fig. 2). For $\overline{\sigma}>0$ the correlation function decreases monotonically as q increases from zero.

The appearance of a peak in the displacement correlation function (4), at a finite wave vector q_0, means that there is a characteristic wavelength for the thermal fluctuations. A divergence in the correlation function would correspond to long-range order at that wavelength, while a finite peak corresponds to domains with an intermediate-range order, i.e., enhanced correlations at the lengthscale $1/q_0$. In our case, the domain structure corresponds to regions with varying amplitude of thermal fluctuations. We see in Fig. 3 that the wavelength of these ''fluctuations domains,'' at its minimum,

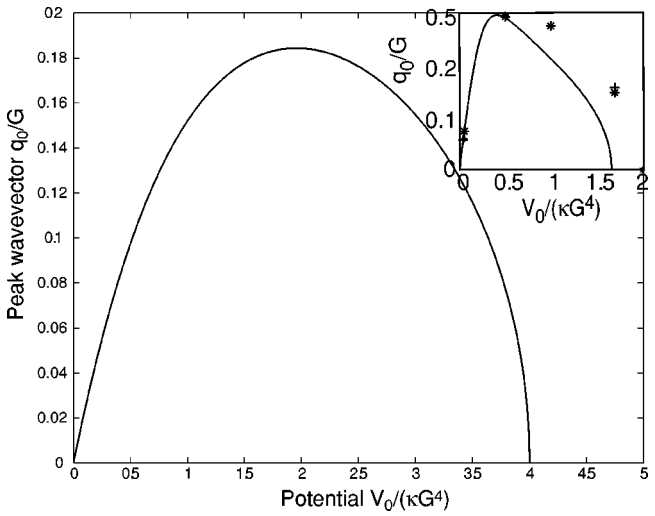

FIG. 3. The approximate analytic expression for the wave vector q_0 [Eq. (A5)] where a peak appears in the correlation function χ_q, for the two-dimensional checkerboard potential. In the inset we compare the analytic and numerical calculation for the one-dimensional sinusoidal potential.

is approximately six times the periodicity of the harmonic potential. Note from Eq. (12) that q_0 is given in terms of the scaling function $Gf(V_0/\kappa G^4)$, since G is the only length scale, and $V_0/\kappa G^4$ is the ratio of the two energy scales in the model.

For small harmonic potentials, the domain wave vector is linear in the potential (A5) $q_0\to G(V_0/4G^4\kappa)$ (Fig. 3). This linear regime bears some resemblance to the intermediate-range order in crystalline (or tethered) membranes above the disclination melting temperature [11]. In such tethered membranes, there is crystalline order over length scales smaller than $r_c\sim\kappa/\mu b$, where μ is the shear modulus of the membrane and b is the length scale of a dislocation. In other words, tethered membranes have enhanced correlations on length scales less than r_c, behaving as an isotropic liquid at longer length scales. If the shear modulus of such a membrane is written in terms of our confining harmonic potential (see the following section) as $\mu\sim V_0/G^2$, and $b\sim 1/G$, we recover $r_c\simeq 1/q_0$. This is the length scale at which the bending (of the bilayer) and stretching (of the tethers) energies balance each other in such membranes. Similarly in our model the periodic potential induces stretching of the membrane, which can be balanced by the bending energy for all $r<r_c$. The balancing of the two opposing forces of stretching and bending, at the wave vector q_0, allows the membrane fluctuations (and correlations) to be enhanced there.

Experimental evidence for enhanced membrane deformations on such length scales is seen in freeze fracture electron micrograph of a RBC membrane [12]. Small undulations with wavelengths of $\sim$100 nm are seen, which is of the order of the distance between neighboring cytoskeleton-bilayer coupling sites, corresponding to our G. A phase with a similar finite (nondivergent) peak in the correlations at a finite wave vector, but with no long-range order or instability (which are both associated with divergent correlations), is seen in microemulsions [13]. In these systems a random

sponge phase exhibits a characteristic length scale for the size of the water-oil domains. Negative surface tension in general can lead to a divergence in the amplitude of thermal fluctuations at some q. In our system the negative surface tension does not lead to a real instability since in the accessible region of q space, there are always the positive curvature κq^4 and confinement γ terms in the Hamiltonian (2), which keep the membrane area fluctuations finite.

We thus find an interplay between three length scales characterized by q_0, G, and $q_c=(\gamma/\kappa)^{1/4}$. The disappearance of the spontaneous structure in the fluctuation spectrum, for large V_0, can be qualitatively understood as follows. When V_0 is large enough, the persistence length of the membrane $\sim 1/q_c$ is smaller than the harmonic potential periodicity. In this case, the confining effect of each harmonic potential peak is effectively decoupled from its neighbor, and there is no emergent intermediate-range order, with length scale $1/q_0$. In other words, the $V_0\to\infty$ limit ''breaks'' the membrane, so that no significant coherence remains on the scale of G^{-1}.

We can also compare our results to those of the crumpling transition in phantom crystalline (or tethered) membranes [14], without self-avoidance. In these studies a continuous transition was found from a flat to a crumpled phase, as the surface tension changes from negative to positive. We find similarly that as the surface tension changes from negative to positive, the wave vector q_0 at which there is a peak in the correlation function vanishes. The ''crumpled'' phase in our case corresponds to $q_0=0$, which means that the membrane conforms to the applied harmonic potential, after averaging. For tethered membranes this corresponds to the regime where the tethering is strong enough to cause crumpling. The ''flat'' phase corresponds in our case to the regime where the persistence length of the membrane is longer than the periodicity of the applied potential, so that an intermediate-range order at a finite $q_0>0$ appears. We find that within our approximation (12) $q_0\propto\sqrt{\sigma}$ as $V_0\to V_c$ (Fig. 3), as was found for the phantom membranes, when the critical point of the crumpling transition is approached from the flat phase [14].

IV. CYTOSKELETON OF THE RBC

We now wish to compare the results of our model to the experimentally well studied case of the RBC (Fig. 1). The cytoskeleton of the RBC is a two-dimensional (roughly) triangular network made up of flexible spectrin molecules, attached at their ends to actin complexes, and through them to the lipid bilayer [1]. The length of the spectrin connections of the network is $\sim$100 nm, while the size of the regions coupling the cytoskeleton to the bilayer is $\sim$10 nm [1], thus forming a sparse (dilute) confinement (Fig. 1). The spectrins are further attached to the membrane at random sites along their length by ankryn molecules. The spectrins behave as entropic springs and give the cytoskeleton a shear modulus of $\mu\sim 6\times 10^{-6}$ J/m^2 [15].

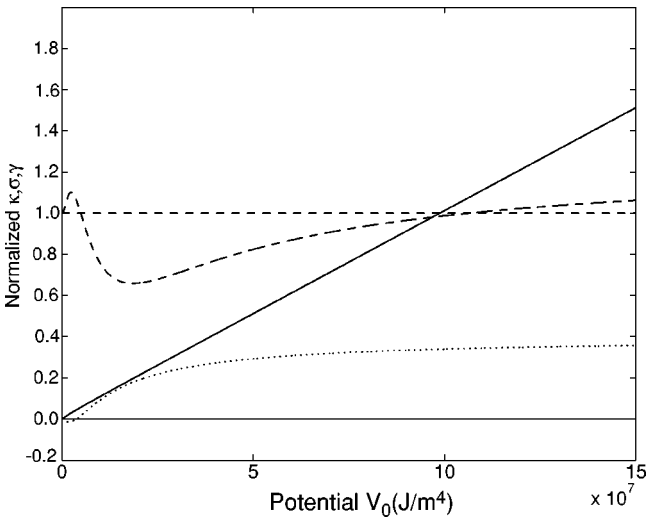

FIG. 4. The calculated elastic parameters $\overline{\gamma},\overline{\kappa}$, and $\overline{\sigma}$ as a function of the potential V_0, for $G=1/380$ nm^{-1}. We normalize the parameters by the measured values γ_{ex}, κ_{ex}, and σ_{ex}, respectively, for the first RBC of Table I. It is clear that both $\overline{\gamma}$ and $\overline{\kappa}$ approximately agree with the measured values at $V_0\sim 10^8$ J/m^4, while $\overline{\sigma}$ at most approaches $\sim\sigma_{ex}/3$.

We have previously [5] analyzed the measured spectrum of the thermal fluctuations of the RBC membrane [16], and found phenomenologically that it can be described using the three parameters κ,σ,γ as in Eq. (A3). In the present work we compare these phenomenological parameters with the results of our microscopic model (11), which highlights the effects of the inhomogeneous coupling of the cytoskeleton to the lipid membrane. Through the results of our model of the preceding section, these parameters, namely $\overline{\gamma},\overline{\sigma},\overline{\kappa}$, are shown to be related to the physical properties of the cytoskeleton, namely G,V_0.

We find the values of G,V_0 which give $\overline{\gamma}\simeq\gamma_{ex}$ and $\overline{\kappa}\simeq\kappa_{ex}\sim 2\times 10^{-20}$ J (Fig. 4), and are given in Table I (for the two extreme examples of measured RBC's). Note that the approach to the asymptotic value $\overline{\kappa}=5\kappa/4$ is very slow (Figs. 2 and 4).

We find in both cases that the predicted surface tension $\overline{\sigma}$ is smaller than the measured value σ_{ex} by a factor of $\sim$3 (Table I and Fig. 4). The calculated surface tension is close to the asymptotic value of strong confinement $\overline{\sigma}\sim 2\kappa G^2$ (11). Note also that this value is $\sim\mu/30$, but is still much larger (two orders of magnitude) than the surface tension arising from area conservation of the RBC [5]: $\sigma_0=\kappa/R^2\sim 1\times 10^{-9}$ J/m^2 (taking $R\sim 4$ μm for the RBC radius). The fac-

TABLE I. Values of G, V_0 which give $\overline{\gamma}\simeq\gamma_{ex}$ and $\overline{\kappa}\simeq\kappa_{ex}\sim 2\times 10^{-20}$ J.

$V_0\times 10^8$ (J/m^4)	G(nm^{-1})	$\epsilon^{-1}=V_0/\kappa G^4$	G/q_c	$\gamma_{ex}\times 10^7$ (J/m^4)	$\sigma_{ex}\times 10^{-7}$ (J/m^2)
1	1/380	104	2.5	7.5	7
0.13	1/650	116	3	1	2.8

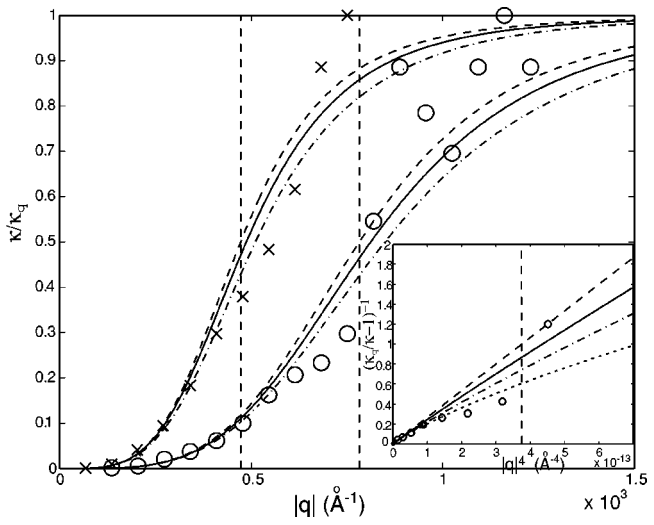

FIG. 5. Comparison of the calculated $\kappa_q = 1/(q^4 \chi_q)$ for the two-dimensional checkerboard potential, Eq. (A3) (taking $V_1 = V_0$)—solid lines; a one-dimensional sinusoidal potential [Eq. (A9)]—dash-dot lines and measured (symbols) for the two RBC's of Table I. The two fitting parameters are G and V_0. The simple fit without surface tension (only average confinement γ) is shown as dashed lines, while the wave vector $q_c \sim (\gamma/\kappa)^{1/4}$ is indicated by the vertical dashed lines. The inset shows the data for one of the cells, so that the importance of the large effective surface tension for $q \lesssim q_c$ is apparant. The calculated surface tension $\bar{\sigma}$ is seen to be smaller than the experimentally measured value σ_{ex} (dotted line).

tor of 3 discrepancy can be attributed to the fact that we chose a particularly simple model with a single sine wave modulation, with $V_0 = V_1$. Note in Table I that the measurements on two different cells also differ by about a factor of 3.

The significant result is that the cytoskeleton-induced tension is two orders of magnitude larger than the tension due to area conservation. The surface tension imposed by the periodic potential is therefore distinct from both the cytoskeleton shear strength and the area conservation condition.

We now relate the values of G and V_0 to the microscopic structure of the RBC cytoskeleton. The calculated periodicity of the sinusoidal potential in Table I is of the order of the observed average distance between cytoskeleton-bilayer connection sites [2] ($\sim$150 nm). Additionally, the values of the peak confining harmonic potential exerted by the cytoskeleton $V_0 \sim 100 \kappa G^4$ can be related to the shear strength per unit area of the cytoskeleton μ: $V_0 \sim \mu G^2 \simeq (0.14\text{–}0.4) \times 10^8$ (J/m^4). The strength of the confining potential that the cytoskeleton exerts on the lipid membrane at the coupling site is related to the cytoskeleton stiffness. This is so because it is only the local shape changes of the cytoskeleton that provide a restoring force to the fluctuations of the lipid membrane, above and beyond its intrinsic bending modulus κ (Fig. 1). The relatively large difference between the two cells above can be due to natural variations in the structural properties of the cytoskeleton. For example, the density of ankryn may vary [17], and with it the entropic stiffness of the spectrin network.

We now compare the behavior at all wave vectors. In Fig. 5 we compare the observed and the calculated effective bending modulus $\kappa_q \equiv 1/(q^4 \chi_q)$, using Eq.(A3) with $V_1 = V_0$. We find that both the two-dimensional model with a checkerboard potential and the one-dimensional sinusoidal potential can reproduce fairly well the low q behavior, including the appearance of the relatively large effective surface tension. The measured data, though, show a more abrupt change around the crossover wave vector q_c (vertical dashed lines in Fig. 5) [18,19]. This is likely due to the more discrete nature of the cytoskeleton-bilayer coupling, which is not captured by the smooth sinusoidal potential. The comparison between the one-dimensional and two-dimensional calculation emphasizes the dependence of the emergent elastic parameters κ, σ, and γ on the details of the symmetry and geometry of the harmonic potential, which in the RBC has a mixed hexagonal-pentagonal symmetry. Note that the importance of the induced surface tension is apparent only for wave vectors smaller than the crossover $q \lesssim q_c$ (Inset of Fig. 5). We see again that the calculated surface tension $\bar{\sigma}$ is too small ($\sim \sigma_{ex}/3$).

Although the coupling of the cytoskeleton to the membrane occurs at distinct sites (Fig. 1), the checkerboard model gives a surprisingly good approximation of the real cytoskeleton-bilayer coupling in the RBC, because of the fluctuations of these coupling points. Looking at a schematic picture of the membrane, we can see that the cytoskeleton strongly confines the bilayer over an actin patch of $\sim$30 nm in diameter (Fig. 1). The spectrin molecules, which form the links of the cytoskeleton network, emanate from such a patch. The bilayer-spectrin separation therefore increases radially as one moves away from the connecting patch, with a gradual consequent decrease in the confining strength [20]. In addition, the position of the connecting patch thermally fluctuates in the liquid bilayer [21], with an observed amplitude of $\sim$20 nm. This further smooths the effective confinement of the bilayer by the cytoskeleton, and explains why the effective periodicity we find by fitting to our model [Table I] is larger than the static periodicity.

V. PERIODIC δ POTENTIALS

In this section we examine the case of a highly localized cytoskeleton-bilayer coupling, in the form of a periodic series of δ functions. This corresponds to the opposite limit of the smooth sinusoidal variation examined above. Physically this scenario corresponds to a rigid and stiff cytoskeleton, highly separated from the bilayer, except at the points of contact.

To obtain analytic solutions we limit ourselves to the one-dimensional case, which we compare with a similar calculation of the sinusoidal variation (end of Appendix A). In one dimension Eq. (5) becomes

$$V \sum_m \left[\delta(x - a(m-1)) + \delta(x - am) \right] \chi(x) + \kappa \frac{\partial^4 \chi(x)}{\partial x^4} = f \delta(x) \tag{13}$$

with the δ functions at positions $x = am$ and strength V in units of J/m^3). We parametrize the solution for each section

of coordinate $a(m-1)\leqslant x\leqslant am$ by the exact solution of Eq. (13) in the regions between each of the δ functions:

$$\chi_m(x)=\alpha_m+\beta_m x'+\gamma_m x'^2+\epsilon_m x'^3, \tag{14}$$

where $x'=x-(m-1)a$. We then write the boundary conditions for each section, which are the continuity conditions for the functions $\chi,\partial\chi/\partial x,\partial^2\chi/\partial x^2$:

$$\gamma_m-\gamma_{m-1}=3a\epsilon_{m-1},$$

$$\beta_m-\beta_{m-1}=2a\gamma_{m-1}+3a^2\epsilon_{m-1},$$

$$\alpha_m-\alpha_{m-1}=a\beta_{m-1}+a^2\gamma_{m-1}+a^3\epsilon_{m-1}. \tag{15}$$

The fourth equation we need is given by the integration of Eq. (13)

$$\epsilon_m-\epsilon_{m-1}=-\frac{V}{6\kappa}\alpha_m+\frac{f}{6\kappa}\delta_{m,1}, \tag{16}$$

where the last term accounts for the applied force at the origin.

We now perform a discrete Fourier transform of these equations, and solve Eq. (B1), to find $\alpha_q,\beta_q,\gamma_q,\epsilon_q$ (Appendix B). Using the solution of Eq. (B1) in Eq. (B2) (Appendix B) we finally find

$$\chi_q=\frac{f}{\kappa q^4+\gamma},$$

$$\gamma=\frac{16a^3q^4V[2+\cos(aq)]\sin(aq/2)^4}{3|-1+e^{iaq}|^8}, \tag{17}$$

which for small q has the form

$$\gamma\simeq\frac{V}{a}+\frac{a^3V}{720}q^4 \tag{18}$$

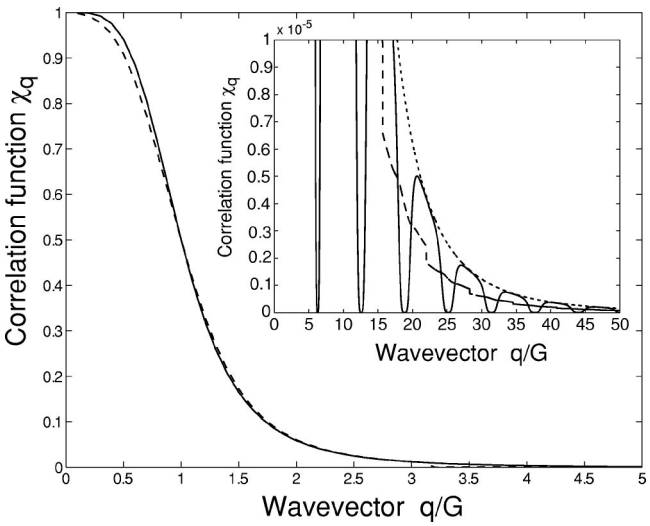

FIG. 6. The calculated correlation function χ_q (solid line) for a one-dimensional periodic array of harmonic δ functions [Eq. (17)] and for the position-averaged case [Eq. (19), dashed line]. In the inset we plot these functions for larger q values, compared with the approximate expression (18) (dotted line). Note that the spatial averaging of the potential removes the oscillations.

and amounts to a uniform confinement combined with a renormalization of the curvature bending modulus. Note the absence of a surface tension term in this case, in contrast to the sinusoidal potential (A11). As expected, the infinitely strong coupling at the positions of the δ functions introduces zero response at the corresponding wave vectors $q=2\pi n/a$ $(n=0,1,2\ldots)$, where $\gamma\to\infty$ (Fig. 6).

To take into account the averaging over the relative position of the δ-function harmonic potentials and the origin, the potential V in Eq. (17) gets multiplied by a phase factor $e^{i\delta q}$, with $-a<\delta<a$. Integrating over this phase,

$$\chi_q=\frac{f}{2a\kappa q^5}\left(aq+2\arctan\left[\frac{\{3\kappa|-1+e^{iaq}|^8-a^3V[8-9\cos(aq)+\cos(3aq)]\}\tan(aq/2)}{3\kappa|-1+e^{iaq}|^8+16a^3V[2+\cos(aq)]\sin(aq/2)^4}\right]\right) \tag{19}$$

and expanding in the limit of small wavevector,

$$f\chi_q^{-1}\simeq\frac{V}{a}+\frac{aVq^2}{6}+\left(\kappa+\frac{Va^3}{48}\right)q^4. \tag{20}$$

We find that the averaging process leads to the appearance of a positive surface tension term $\sigma_\delta\simeq aV/6$, while the nodes in the correlation function disappear (Fig. 6). Comparing with the previous sections, we find that $\sigma_\delta\sim\mu(aG)^2/6$, so that the calculated surface tension can be related to the shear modulus of the cytoskeleton μ, but is smaller by about an order of magnitude. Notice the difference between the expressions for the surface tension in the case of a sinusoidal potential [Eq. (11)] and σ_δ. In particular, there is no dependence on the curvature bending modulus κ in the latter case. The dependence on the confining potential V is quadratic in the former, while it is linear in the case of periodic δ potentials.

As we discussed in the end of the preceding section, the actual confining potential in the RBC is most probably smooth, rather than a δ-function-like potential. This is despite the fact that the cytoskeleton is strongly attached to the membrane at confined sites (Fig. 1). The position of these patches thermally fluctuates in the liquid bilayer [21], with

an observed amplitude of ~20 nm. This smooths the effective confinement interaction of the bilayer and the cytoskeleton.

VI. CONCLUSIONS

In this work we described analytical and numerical results for models of inhomogeneous (periodic) harmonic confinements of fluid membranes. These models are applied to experiments that are sensitive to the physical coupling between the cellular cytoskeleton and outer lipid membrane. Our results show that a smooth inhomogeneous potential "pulling" on the liquid membrane causes a spontaneous surface tension, and uniform confinement, to appear. The calculation presented here provides a microscopic justification for the phenomenological model previously introduced [5], which provides a unified description of both the static and dynamic spectrum of the RBC membrane fluctuations.

Positive tension acts to suppress the thermal fluctuations, as observed in the membrane of the RBC. The emergent tension turns out to be negative for weak potentials (or large periodicity), signaling the appearance of intermediate-range order (domains) in the membrane thermal fluctuations. This surprising result may be more quantitatively tested using artificial vesicles or genetically manipulated RBC.

Our results point the way to an effective elastic description of composite membranes containing a bilayer and an attached cytoskeleton, such as in the RBC. This should have implications not only for the fluctuation spectra, as we have discussed, but also for the overall shape and large-scale deformations (as in tight capillaries).

ACKNOWLEDGMENTS

This work was supported by an ISF grant. The authors are grateful to the donors of the Petroleum Research Fund administered by the American Chemical Society, the Schmidt Minerva Center, and BSF Grant No. 183-2002 for their support. N.G.'s research was supported by the Koshland Foundation.

APPENDIX A

We give in this appendix the detailed calculations of the expressions in Sec. II.

We begin with the exact result for the real-space height-height correlation function of a free membrane, in the limit of infinite membrane $L\to\infty$,

$$\langle h(0)h(r)\rangle \simeq \frac{k_BT}{\kappa}\left[\frac{\pi}{2}r^2\log\left(\frac{\pi L}{r}\right)+\frac{L^2}{4\pi}+\frac{\pi}{2}r^2[\Gamma-1]\right], \tag{A1}$$

where $\Gamma=1.154\,33$ is the Euler-Gamma number.

Similarly, for a uniformly confined membrane

$$r\to\infty:\langle h(0)h(r)\rangle\to 0,$$

$$r\to 0:\langle h(0)h(r)\rangle=\frac{k_BT}{8\sqrt{\kappa\gamma}}, \tag{A2}$$

where the $r\to\infty$ limit shows that the confining effect screens the long wavelength fluctuations, while the limit $r\to 0$ gives a size-independent mean square displacement (9).

We next give here a cut through the full solution χ_q of Eq. (10) of a two-dimensional checkerboard potential, along the q_x axis (i.e., $q_y=0$). We take $V_1=V_0$, so that the harmonic potential vanishes at the minima, and average over the phase of the sinusoidal potential (δ_x,δ_y):

$$\begin{aligned}\chi_{q_x,q_y=0}=f\{&4[16G^8\kappa^2+16G^2\kappa q_x^2V_0+8G^4\kappa(\kappa q_x^4+V_0)\\&+(\kappa q_x^4+V_0)^2]\}/[4\kappa^3q_x^{12}+12\kappa^2q_x^8V_0+11\kappa q_x^4V_0^2\\&+3V_0^3+64G^8\kappa^2(\kappa q_x^4+V_0)+8G^2\kappa q_x^2V_0(8\kappa q_x^4\\&+7V_0)+4G^4\kappa(8\kappa^2q_x^8+16\kappa q_x^4V_0+7V_0^2)].\end{aligned} \tag{A3}$$

This complicated expression has the correct $q\to\infty$ dependence, namely $\chi_{q_x}\to f/(\kappa q_x^4)$. For the behavior at small q_x, we expand f/χ_{q_x} up to fourth order in q_x, with the coefficients given in terms of the dimensionless parameter $\epsilon\equiv G^4\kappa/V_0$:

$$\frac{f}{\chi_{q_x}}\simeq\bar{\gamma}+\bar{\sigma}q_x^2+\bar{\kappa}q_x^4,$$

$$\bar{\gamma}=V_0\frac{16\epsilon+3}{4(4\epsilon+1)},$$

$$\bar{\sigma}=2G^2\kappa\frac{(-4\epsilon+1)}{(4\epsilon+1)^3},$$

$$\bar{\kappa}=\kappa\frac{(4096\epsilon^5+5120\epsilon^4+2624\epsilon^3+1200\epsilon^2-36\epsilon+5)}{4(4\epsilon+1)^5}. \tag{A4}$$

For the range of small harmonic potential $V_0<4\kappa G^4$, we find a peak in χ_{q_x} (A3), at the wave vector

$$q_0=\frac{2GV_0\sqrt{-4G^4\kappa+V_0}}{\left(-\dfrac{16384G^{20}\kappa^5+19456G^{16}\kappa^4V_0+9472G^{12}\kappa^3V_0^2+4144G^8\kappa^2V_0^3-152G^4\kappa V_0^4+15V_0^5}{(4G^4\kappa+V_0)(16G^4\kappa+3V_0)}\right)^{1/2}}. \tag{A5}$$

We now give two simpler cases which we calculated. The first is a two-dimensional calculation of a single sinusoidal harmonic potential in the x direction. Similar to Eq. (10), we can write

$$[V_1+\kappa(q_x^2+q_y^2)^2]\chi_q+\frac{V_0}{2}e^{i\delta}\chi_{G+q}+\frac{V_0}{2}e^{-i\delta}\chi_{-G+q}=f,$$

$$\frac{V_0}{2}e^{-i\delta}\chi_q+\{V_1+\kappa[(G+q_x)^2+q_y^2]^2\}\chi_{G+q}=f,$$

$$\frac{V_0}{2}e^{i\delta}\chi_q+\{V_1+\kappa[(-G+q_x)^2+q_y^2]^2\}\chi_{-G+q}=f. \tag{A6}$$

The shift of the sinusoidal function with respect to the origin (where the force f is applied), $0<\delta<2\pi$, is again averaged over, giving the result for χ_q (taking $V_1=V_0$):

$$\chi_q=f\{G^8\kappa^2+4G^6\kappa^2(-q_x^2+q_y^2)+[\kappa(q_x^2+q_y^2)^2+V_0]^2+2G^4\kappa[\kappa(3q_x^4-2q_x^2q_y^2+3q_y^4)+V_0]$$
$$+4G^2\kappa[-\kappa(q_x^2-q_y^2)(q_x^2+q_y^2)^2+(3q_x^2+q_y^2)V_0]\}\Big/\Big[-\frac{1}{4}V_0^2\{\kappa[(G+q_x)^2+q_y^2]^2+V_0\}+\{\kappa[(G-q_x)^2+q_y^2]^2+V_0\}$$
$$\times\Big(-\frac{1}{4}V_0^2+[\kappa(q_x^2+q_y^2)^2+V_0]\{\kappa[(G+q_x)^2+q_y^2]^2+V_0\}\Big)\Big]. \tag{A7}$$

Finally, we also calculated the rather artificial case of a one-dimensional membrane with a single sinusoidal harmonic potential. This was useful for detailed comparison with the numerical solution, at higher resolution than was possible for the two-dimensional cases described above. It is also useful for comparison with the case of a periodic array of δ-potentials (Sec. IV). The system of equations is given by

$$(V_1+\kappa q^4)\chi_q+\frac{V_0}{2}e^{i\delta}\chi_{G+q}+\frac{V_0}{2}e^{-i\delta}\chi_{-G+q}=f,$$

$$\frac{V_0}{2}e^{-i\delta}\chi_q+[V_1+\kappa(G+q)^4]\chi_{G+q}=f,$$

$$\frac{V_0}{2}e^{i\delta}\chi_q+[V_1+\kappa(-G+q)^4]\chi_{-G+q}=f. \tag{A8}$$

The solution of χ_q is given by

$$\chi_q=2f[G^8\kappa^2-4G^6\kappa^2q^2-4G^2\kappa q^2(\kappa q^4-3V_1)+(\kappa q^4+V_1)^2+2G^4\kappa(3\kappa q^4+V_1)]/[2G^8\kappa^2(\kappa q^4+V_1)$$
$$-8G^6\kappa^2q^2(\kappa q^4+V_1)+(\kappa q^4+V_1)(2\kappa^2q^8-V_0^2+4\kappa q^4V_1+2V_1^2)+G^4\kappa(12\kappa^2q^8-V_0^2+16\kappa q^4V_1+4V_1^2)$$
$$+2G^2\kappa q^2(-4\kappa^2q^8-3V_0^2+8\kappa q^4V_1+12V_1^2)]. \tag{A9}$$

For the behavior at small q, we expand f/χ_q up to fourth order in q:

$$\overline{\gamma}=\frac{2V_1(\kappa G^4+V_1)-V_0^2}{2(\kappa G^4+V_1)},$$

$$\overline{\sigma}=\frac{G^2\kappa V_0^2(-5\kappa G^4+3V_1)}{(\kappa G^4+V_1)^3},$$

$$\overline{\kappa}=\{\kappa[2G^{20}\kappa^5+10G^{16}\kappa^4V_1-5G^{12}\kappa^3(7V_0^2-4V_1^2)+5G^4\kappa V_1^2(-13V_0^2+2V_1^2)+V_1^3(V_0^2+2V_1^2)+5G^8\kappa^2V_1(31V_0^2$$
$$+4V_1^2)]\}/2(\kappa G^4+V_1). \tag{A10}$$

In the case that the harmonic potential vanishes at the minima ($V_1=V_0$), we get simpler expressions in terms of the dimensionless parameter ϵ,

$$\overline{\gamma}=V_0\frac{2\epsilon+1}{2\epsilon+2},$$

$$\overline{\sigma}=G^2\kappa\frac{(-5\epsilon+3)}{(\epsilon+1)^3},$$

$$\overline{\kappa}=\kappa\frac{(2\epsilon^5+10\epsilon^4-15\epsilon^3+175\epsilon^2-55\epsilon+3)}{2(\epsilon+1)^5}. \tag{A11}$$

APPENDIX B

We now perform a discrete Fourier transform of Eqs. (13)–(16) (on the lattice sites $x=ma$),

$$\sum_m e^{iqma}(\gamma_m-\gamma_{m-1})=\gamma_q(1-e^{iqa})=3a\epsilon_q e^{iqa},$$

$$\beta_q(1-e^{iqa})=2a\gamma_q e^{iqa}+3a^2\epsilon_q e^{iqa},$$

$$\alpha_q(1-e^{iqa})=a\beta_q e^{iqa}+a^2\gamma_q e^{iqa}+a^3\epsilon_q e^{iqa},$$

$$\epsilon_q(1-e^{iqa})=-\frac{V}{6\kappa}\alpha_q+\frac{f}{6\kappa}e^{iqa}. \tag{B1}$$

Solving the system of equations (B1), we find $\alpha_q,\beta_q,\gamma_q,\epsilon_q$. In order to relate this to the Fourier transform of $\chi_m(x)$ we calculate the correlation function χ_q,

$$\chi_q=\sum_m\int_{(m-1)a}^{ma}e^{iqx}\chi_m(x)dx=\alpha_q\frac{(1-e^{iqa})}{iq}+\beta_q\frac{(1-iqa-e^{iqa})}{q^2}+\gamma_q\frac{[2qa+2i(-e^{iqa})-ia^2q^2]}{q^3}$$
$$+\epsilon_q\frac{[-6(1-e^{iqa})+6iaq+3a^2q^2-ia^3q^3]}{q^4}. \tag{B2}$$

[1] V. Bennett, Biochim. Biophys. Acta **988**, 107 (1989).

[2] A. Zilker, H. Engelhardt, and E. Sackmann, J. Phys. I **48**, 2139 (1987); H. Strey, M. Peterson, and E. Sackmann, Biophys. J. **69**, 478 (1995).

[3] S. Tuvia, S. Levin, A. Bitler, and R. Korenstein, J. Cell Biol. **141**, 1551 (1998); S. Levin and R. Korenstein, Biophys. J. **60**, 733 (1991).

[4] M.A. Peterson, Phys. Rev. A **45**, 4116 (1992).

[5] N. Gov, A. Zilman, and S. Safran, Phys. Rev. Lett. **90**, 228101 (2003).

[6] S. A. Safran, *Statistical Thermodynamics of Surfaces, Interfaces and Membranes*, Frontiers in Physics Vol. 90 (Addison-Wesley, Reading, MA, 1994).

[7] D.E. Discher and P. Carl, Cell. Mol. Biol. Lett. **6**, 593 (2001).

[8] C. Kittel, *Introduction to Solid State Physics* (Wiley, New York, 1971), Chap. 9.

[9] Note that similar surface tension of a bilayer due to coupling with an adsorbed polymer layer, has been recently calculated by T. Bickel and C.M. Marques, Eur. Phys. J. E **9**, 349 (2002).

[10] M. Laradji, Europhys. Lett. **60**, 594 (2002); C. Hiergeist and R. Lipowsky, J. Phys. II **6**, 1465 (1996).

[11] D.R. Nelson and L. Peliti, J. Phys. I **48**, 1085 (1987).

[12] A.G. Petrov, S.A. Swleznev, and A. Derzhanski, Acta Phys. Pol. A **55**, 385 (1979).

[13] *Micelles, Membranes, Microemulsions and Monolayers*, edited by W. M. Gelbart, A. Ben-Shaul, and D. Roux (Springer-Verlag, New York, 1994), Chaps. 7–9.

[14] M.J. Bowick and A. Travesset, Phys. Rep. **344**, 255 (2001).

[15] D. Discher, N. Mohandas, and E.A. Evans, Science **266**, 1032 (1994); V. Heinrich, K. Ritchie, N. Mohandas, and E. Evans, Biophys. J. **81**, 1452 (2001).

[16] A. Zilker, H. Engelhardt, and E. Sackmann, J. Phys. I **48**, 2139 (1987); S. Tuvia, S. Levin, A. Bitler, and R. Korenstein, J. Cell Biol. **141**, 1551 (1998); S. Levin and R. Korenstein, Biophys. J. **60**, 733 (1991).

[17] A.F. Sikorski, B.H. Lorenz, A. Jezierski, and A.R. Dluzewski, Acta Biochim. Pol. **47**, 565 (2000).

[18] See also C.F. Schmidt, *et al.*, Science **259**, 952 (1993).

[19] J-B. Fournier, D. Lacoste, and E. Raphaël, Phys. Rev. Lett. (to be published), e-print cond-mat/0306736.

[20] M. Breidenich, R.R. Netz, and R. Lipowsky, Europhys. Lett. **49**, 431 (2000); R. Lipowsky, H-G. Dobereiner, C. Hiergeist, and V. Indrani, Physica A **249**, 536 (1998).

[21] J.C-M. Lee and D.E. Discher, Biophys. J. **81**, 3178 (2001).